INT. J. REMOTE SENSING, 20 SEPTEMBER, 2004,
VOL. 25, NO. 18, 3745–3768

Taylor & Francis
Taylor & Francis Group

Rock unit discrimination on Landsat TM, SIR-C and Radarsat images using spectral and textural information

P. DONG*

Department of Geology, University of New Brunswick, Fredericton, New Brunswick, E3B 5A3, Canada

and B. LEBLON

Faculty of Forestry and Environmental Management, University of New Brunswick, Fredericton, New Brunswick, E3B 6C2, Canada; tel: (506) 453-4924; fax: (506) 453-3538; e-mail: bleblon@unb.ca

(*Received 1 November 2001; in final form 14 July 2003*)

Abstract. The paper presents results for spectral and textural analysis of the rock units in Landsat Thematic Mapper (TM) images, dual-band (L and C) and dual-polarization (HH and HV) Shuttle Imaging Radar (SIR)-C images, and C-band HH polarization Standard Beam 4 and Extended High Incidence Beam 3 Radarsat images from a study area between California and Arizona, USA. Fractal dimension, lacunarity and grey-level co-occurrence matrix (GLCM) textural feature images were created from the SIR-C and Radarsat images. Fractal dimensions were calculated using a differential box counting method and lacunarity measures were obtained using a new grey-scale lacunarity estimation method for 36 sample images extracted from the SIR-C and Radarsat images. The fractal dimension and lacunarity curves and class signature separability analysis show that, for rock unit discrimination using image textural features in the study area, the SIR-C L-HH image is more suitable than other SIR-C images and Radarsat images, and that co-polarization (HH) generally provides more textural information than cross-polarization (HV) in the study area. The study also shows that lacunarity measures can reveal the scaling properties of radar image textures for rock units. The combination of spectral information from Landsat TM images and textural information from radar images improves the image classification accuracy of rock units in the study area.

1. Introduction

Since the 1930s, aerial photographs in the visible spectral region have been utilized for interpreting geological features (Nowhuys 1937, Melton 1945, Desjardins 1950, Miller 1961). While visible aerial photographs make it possible for geological mapping in areas where field investigation is difficult due to poor accessibility, they do have drawbacks: (1) they only provide information of objects in the visible band; (2) their acquisition depends on the weather; and (3) they are

*Corresponding author. Current address: CIESIN, Columbia University, 61 Route 9W, PO Box 1000, Palisades, NY 10964, USA; e-mail: pdong@ciesin.columbia.edu

International Journal of Remote Sensing
ISSN 0143-1161 print/ISSN 1366-5901 online
http://www.tandf.co.uk/journals
DOI: 10.1080/01431160310001632675

normally recorded in analogue format, which precludes quantitative analysis. Many traditional aerial photographic systems have been replaced by airborne and space-borne electro-optical (visible, reflected infrared and thermal infrared) and electronic (radar) sensor systems since the late 1960s and early 1970s. Visible and reflected infrared, and thermal infrared images provide much more information than visible aerial photographs on the spectral properties of rocks and minerals, and greatly facilitate the application of remote sensing to geological mapping and mineral exploration. However, images from electro-optical systems are still hindered by cloud cover and Sun illumination conditions. The limitation can be removed by radar imaging systems that operate independently of lighting conditions and largely independently of weather.

The electro-optical and radar images in digital format allow for quantitative analysis. For digital image processing, spectral analysis of multispectral images concentrates on individual pixel locations, while textural features contain information on the spatial arrangement of tonal values within an image. Although spectral analysis can be very effective in discriminating different features in the image, it has limitations in some cases. For example, spectral analysis methods may not be able to discriminate sandstones from shales due to the similar spectral properties of the two rock types, but texture analysis may be able to discriminate the two rock types because sandstones normally have a coarser textured drainage pattern than shales (Sabins 1987). Many studies in remote sensing of renewable natural resource have shown that combination of spectral and textural features can improve the classification accuracy (table 1). For rock unit discrimination, there are a lot of studies using remotely sensed spectral data (e.g. Kahle and Goetz 1983, Greenbaum 1987, Sabins 1987, Vandermeer 1996), but only a few number of studies have been carried out to compare spectral with textural analysis of images (table 1). In radar image analysis, texture is an important image element which may be equally important as spectral dimension (Simonett and Davis 1983), or even more useful than spectral dimension (Ulaby *et al*. 1986). Spectral analysis methods such as per-pixel classifiers that were successful with Landsat images yield poor results when applied to radar images, due in part to the presence of coherent fading (or speckle) in the radar image (Ulaby *et al*. 1986). Unlike visible and reflected-infrared waves, which interact matters on the molecular scale, microwaves from radar systems interact with the Earth's surface on the scale of radar wavelength (1–100+ cm). Accordingly, direct mapping of rock units based on composition is not possible with radar images (Elachi 1982). However, the surface morphology of rock units is often related to the composition and weathering characteristics of the rocks. It is therefore possible to discriminate different rock units using their image textural patterns. This is particularly true for radar images, because of the sensitivity of radar backscatter to local topographic slopes.

In the past decades, many textural analysis methods have been published for various application purposes. For geological applications, statistical textural analysis methods, particularly the grey-level co-occurrence matrix (GLCM) based measures proposed by Haralick *et al*. (1973), are the most popular ones (Weszka *et al*. 1976, Shanmugam *et al*. 1981, Blom and Daily 1982, Gaddis *et al*. 1989, 1990, Wang and He 1990). These geological case studies used visual interpretation of texture images (for example, Gaddis *et al*. 1989, 1990), or scatter diagrams of textural features (for example, Shanmugam *et al*. 1981, Wang and He 1990), for detection of different rock unit textures. In recent years, there are a few studies that have incorporated texture features into the classification of rock units. Mather *et al*.

Table 1. Examples of literature results on comparison between spectral and spectral + textural analysis, in terms of percentage of correct classification for the considered features.

Detected features	Sensor	Time of the year	Location	Textural parameter(1)	% correct classification		Authors
					Spectral	Spectral + Textural	
Landuse and landcover	Landsat MSS	July	Oakland (USA)	8	74.0–77.7	83.5	Haralick and Shanmugam (1974)
	SPOT	August	Toronto (Canada)	1, 2, 3, 4, 5	0.574(2)	0.665(2)	Gong *et al.* (1992)
	Landsat TM	July	Cukurova Deltas (Turkey)	9, 10	74.0	89.0	Berberoglu *et al.* (2000)
	ERS-1 SAR, JERS-1 SAR		Finnish Lapland (Finland)	1, 2, 3, 4	50.0	65.0	Kurvonen and Hallikainen (1999)
Forest and urban areas	MEIS-II	August	Montréal (Canada)	6	82.0	94.0	Anys *et al.* (1994)
Various forest and non forest areas	SPOT-HRV PLA	October	Bonaventure (Canada)	2, 3, 4, 5	9.0–63.0(3)	40.0–100.0(3)	Marceau *et al.* (1990)
Forest cover types	Landsat MSS	July	Gros Morne National Park (Canada)	2	59.1	66.2	Franklin and Peddle (1989)
	SPOT-HRV MLA	August	Gros Morne National Park (Canada)	2, 3	51.1	86.7	Franklin and Peddle (1990)
	SPOT-HRV MLA	August	Gros Morne National Park (Canada)	4	73.2	87.8	Peddle and Franklin (1991)
	Landsat TM	August	Chatham (Canada)	1	34.2	39.5	Prihatno (1995)
Clearcut	Landsat TM	August	Chatham (Canada)	1	69.0	71.0	Prihatno (1995)
	Landsat TM	August	Cranbrook (Canada)	Std(4)	93.0(5) 95.6(6)	96.1(5) 100.0(6)	Arai (1993)
Rock units	Landsat TM and SIR-C C-HH	n/a	Red Sea Hills (Sudan)	1, 2, 11, 12, 13	57.0	70.0	Mather *et al.* (1998)
	Landsat TM	n/a	Almeria (Spain)	10	80.0	83.0–89.0	Chica-Olmo and Abarca-Hernaândez (2000)

(1) Textural parameter: 1 = Homogeneity; 2 = Entropy; 3 = Inverse difference moment; 4 = Angular second moment; 5 = Contrast; 6 = Mean; 7 = Coefficient of variation; 8 = Spatial Grey-Tone Dependence Matrix; 9 = Variance; 10 = Variogram; 11 = Fourier transform; 12 = MAR model; 13 = Multi-fractal.
(2) Kappa coefficients;
(3) Depending on the classified features (fallow land, agricultural fields, residential areas, bare soil, conifers, mixed forest, deciduous, peat bog, quarry);
(4) Std = standard deviation in the band TM4 (more a spatial parameter than a true textural parameter);
(5) New clearcut (confusion with alpine meadows);
(6) Old clearcut.

(1998) employed the Fourier power spectrum, GLCM, multi-fractal measures, and the multiplicative autoregressive random field (MAR) model for texture analysis of Shuttle Imaging Radar (SIR)-C C-band HH polarization image for the discrimination of surface rock types in an arid region, the Red Sea Hills of Sudan. Chica-Olmo and Abarca-Hernaândez (2000) combined variogram measures and Landsat Thematic Mapper (TM) image and obtained improved classification accuracy for three different Quaternary deposit units in a study in Spain. In both studies, inclusion of textural information into the image analysis improved classification accuracy (table 1).

The major disadvantages of the GLCM-based texture analysis are the lack of any compelling theory underlying the texture measures, and the large amount of potential measures. Since the work of Mandelbrot (1977, 1982), fractal geometry has received increased attention as a novel model for natural phenomena. There is evidence that most natural surfaces are spatially isotropic fractals and that intensity images of these surfaces are also fractals (Pentland 1984), which laid the foundation for the use of fractal models in image texture analysis. The geometry of structures grown in many physical processes can be characterized by fractal dimension that can be viewed as a measure of their irregularity (Mandelbrot 1982). However, it becomes apparent that many natural fractal objects are often not very structurally uniform and have variable ranges of self-similarity. For example, very differently looking objects can have the same or very similar fractal dimension (Mandelbrot 1982, Voss 1986, Smith *et al.* 1996, Dong 2000a), and fractal dimension alone would be useless for discriminating these objects.

Mandelbrot (1982) introduced the term lacunarity to describe the characteristic of fractals of the same dimension with different texture appearances, and expected that the 'elusive notion' of texture could be quantified by lacunarity. Following the work by Plotnick *et al.* (1993) on the measurement of simulated binary habitat types in landscape ecology using lacunarity, some researchers have employed lacunarity for texture analysis of forests and ecosystems with remotely sensed images (Kux and Henebry 1994a, b, Henebry and Kux 1995, 1996, Ranson and Sun 1997). It is noticed that all these studies were based on binary images, and grey-scale images had to be sliced into binary images prior to lacunarity analysis. Since the concept of lacunarity is based on fractals and has been extended to non-fractals (Mandelbrot 1982, Allain and Cloitre 1991, Plotnick *et al.* 1993, 1996), it is reasonable to believe that lacunarity should not be limited to binary objects. Moreover, extension of lacunarity estimation to grey-scale images could reveal more valuable textural information than lacunarity measure of binary images, mainly because detailed textural information is lost in the process of converting a grey-scale image (for example 8-bit) into a binary image (1-bit). Therefore, there is a need to use new lacunarity estimation methods for grey-scale images.

Voss (1986) proposed a probability method to estimate the lacunarity of grey-scale image intensity surfaces based on the mass of boxes. However, the Voss method used cubic boxes that may not cover image intensity surfaces with sharp variations in pixel values. In an earlier publication (Dong 2000b), a new lacunarity measurement method for grey-scale images was introduced and tested on Brodatz texture patterns (Brodatz 1966). The results of Dong (2000b) showed better performance of the new lacunarity measure in comparison with some statistical-based and fractal-based textural measures, including the fractal dimension, the binary lacunarity, and the grey-scale lacunarity proposed by Voss (1986). In this paper, GLCM, fractal dimension and lacunarity will be employed for analysis of rock unit textures from the dual-band (L and C) and dual-polarization (HH and

HV) SIR-C images and Radarsat standard beam 4 (STDD4) and extended high incidence beam 3 (EXTH3) images in a study area between California and Arizona, USA. Textural information from radar images will be combined with spectral information from Landsat TM images for image classification of rock units. The purposes of this study are twofold: (1) to compare the abilities of the above-mentioned radar images in discriminating different rock unit textures, using conventional statistics, fractal dimension, lacunarity, and class separability analysis results; and (2) to test the performance of the new lacunarity measure in the classification of rock units using spectral and textural information. Fractal dimension estimation was based on a differential box counting method proposed by Sarkar and Chaudhuri (1992), and lacunarity estimations were obtained using a method proposed by Voss (1986) and a new method developed by Dong (2000b) to compare the effectiveness of the two lacunarity estimation methods.

2. Study area and data

The study area is located at the south-easternmost corner of California, covering part of Arizona, USA (figure 1). It lies to the east of the Imperial Valley, and includes part of the Chocolate Mountains, which extend north-westward from the Colorado River. The climate of the region is extremely arid. Rainfall generally ranges between 5–7 cm per year. There is no vegetation cover in the study area except for very small areas in the Colorado River valley. Therefore, influence of soil moisture and vegetation on the radar signal is minimal in the study area. A geological map of scale 1 : 125 000 compiled by Morton (1966) was used as reference for classifying rock units. Rock units of the study area are divided mainly into two groups: Tertiary rocks and undivided Pre-Tertiary rocks (Morton 1977). Major rock types in the study area include quartz biotite gneiss, sericite schist, undivided metasedimentary rocks, sedimentary breccia, volcanic rocks, basalt flows, clastic rocks, and unconsolidated Quaternary sediments. In order to select representative training areas from the rock units for image classification, and to evaluate the classification accuracy quantitatively, the rock units were digitized from the 1 : 125 000 scale geological map (Morton 1966), and converted into ESRI GRID

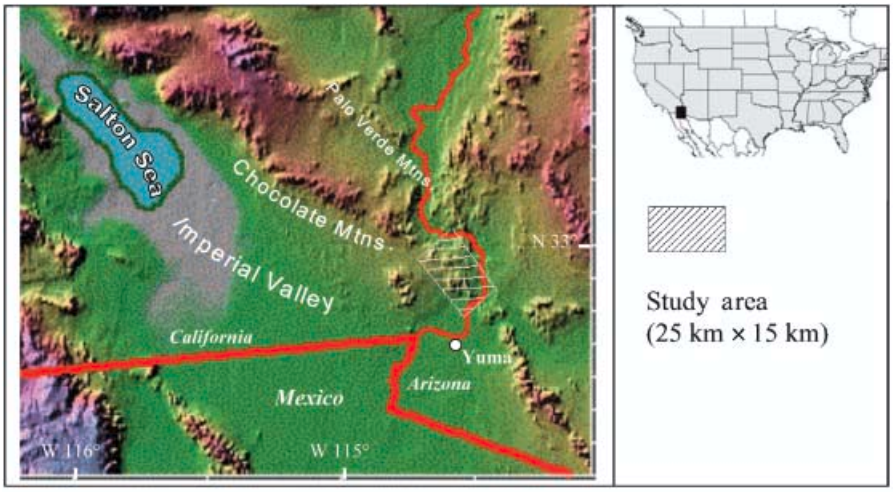

Figure 1. Geographical location of the study area.

format. Each rock unit was assigned a unique value, and an AVENUE script developed by the first author for ArcView GIS (ESRI) was employed to automatically retrieve grid values of random sampling points, which greatly facilitates the classification accuracy assessment.

Radar image data from the SIR-C and Radarsat were used in the study. The SIR-C L-band HH and HV polarization, and C-band HH and HV polarization images were acquired in the space shuttle Endeavor mission STS-59 on 12 April 1994. The scene is one of the 300+ SIR-C test sites around the Earth. A study area of 25 km × 15 km (2000 × 1200 pixels) was extracted from the upper left corner of the scene. Radarsat provides C-band HH polarization images with resolutions from 9 to 100 m at different modes. In this study, two images from STDD4 and EXTH3 were used. Some of the SIR-C and Radarsat image parameters are listed in table 2. The SIR-C and Radarsat images were all converted to 8-bit images to reduce the size of the GLCM and facilitate computer processing. Since the conversion is through linear scaling, it does not modify image texture substantially. To investigate whether the textural information obtained by lacunarity analysis can be combined with spectral information to get better classification results, Landsat TM data acquired on 18 November 1996 were also used in this study. Landsat TM, SIR-C and Radarsat images need to be co-registered in order to perform comparison and classification. The Radarsat images were co-registered to the SIR-C images through the cubic interpolation resampling to retain textural features, and the Landsat TM images were co-registered to the SIR-C images through the nearest neighbour resampling so that the spectral data of Landsat TM images are not modified substantially.

Speckle is an issue related to radar images. Speckle effects are normally removed/reduced if the radar image is used for pixel-by-pixel classification (for example, Blom and Daily 1982, Durand *et al*. 1987, Evans 1988), because speckle may create a statistical distribution with a large standard deviation even in homogeneous areas, thereby causing errors for pixel-by-pixel classifiers. However, this is not the case for textural analysis of the radar images. Any attempt to simply remove speckle from the image is done at the expense of all information about the spatial variability of the target scattering properties (Rignot and Kwok 1993). The study by Dellepiane *et al*. (1991) shows that speckle does not significantly affect textural measurement using fractal dimension, though they did not explain the reason for this. In our paper, the major purpose is to examine the performance of

Table 2. Technical parameters for SIR-C and Radarsat images.

	SIR-C	Radarsat (STDD4*)	Radarsat (EXTH3*)
Imaging date	12 April 1994	5 March 1997	13 February 1997
Orbit direction	Descending	Descending	Descending
Looking direction	Right	Right	Right
Incidence angle at image centre	23.072°	33.6–39.6°	52–58°
Resolution at image centre	25 m	30 m	18–27 m
Pixel size	12.5 m × 12.5 m	12.5 m × 12.5 m	12.5 m × 12.5 m
Bits per pixel	40-bit	16-bit	16-bit
Number of looks	5	4	4
Wavelengths	L (23.5 cm), C (5.8 cm)	C (5.8 cm)	C (5.8 cm)
Polarizations	HH, HV	HH	HH

*STDD4—standard beam 4; EXTH3—extended high incidence beam 3.

lacunarity measures in comparison with other textural measures. Therefore, speckle is not removed.

3. Methodology

Analyses of radar image textures in this study are carried out using two image groups.

3.1. *Sample images*

This group consists of sub-image windows of 79×79 pixels (987.5 m $\times$ 987.5 m on the ground) derived from co-registered SIR-C (L-HH, L-HV, C-HH and C-HV) and Radarsat (STDD4 and EXTH3) images for six rock types—basalt, breccia, clastic, granitic, schist and volcanic—resulting in a total of 36 sub-image windows. Sub-image windows for metasedimentary rocks and Quaternary deposits were not included in this group because: (a) it is difficult to extract a 79×79 pixels (987.5 m $\times$ 987.5 m) sub-image for metasedimentary rocks due to the limited sizes of metasedimentary exposure in the study area; and (b) Quaternary deposits generally distribute in flat areas of the study area, and do not have rich texture expressions on the radar images used in this study. Mean digital number (DN) values and standard deviation around the mean DN values were generated for the sub-images from the SIR-C and Radarsat images. GLCM-based texture measures (homogeneity, contrast, dissimilarity and entropy) are calculated for each sub-image. With the help of a Lacunarity Analysis extension developed by the first author based on ESRI's ArcView GIS software (Dong 2000a), fractal dimension and lacunarity measurements were carried out for the 36 sub-images. Fractal dimension estimation was based on a differential box counting method proposed by Sarkar and Chaudhuri (1992), and lacunarity estimations were obtained using a method proposed by Voss (1986) and a new method developed by Dong (2000b) to compare the effectiveness of the two lacunarity estimation methods.

3.2. *Full scenes*

The group is made up of Landsat TM, SIR-C (L-HH, L-HV, C-HH, C-HV) and Radarsat (STDD4 and EXTH3) images of the study area (1200×2000 pixels, 15 km $\times$ 25 km on the ground), and the textural feature images derived from SIR-C and Radarsat images. The textural feature images were created using the non-directional and directional lacunarity measures obtained using the method proposed by Dong (2000b), the lacunarity estimation method proposed by Voss (1986), the fractal dimension measurements based on differential box counting (Sarkar and Chaudhuri 1992) and some GLCM measures (homogeneity, dissimilarity, contrast and entropy) proposed by Haralick *et al.* (1973). Figure 2 shows the flow chart for investigating the performance of the various spectral and textural image combinations for rock unit discrimination in the study area. These steps in the flow chart are described below.

(a) Texture analysis is carried out for SIR-C and Radarsat images using the above-mentioned texture measures in a 17×17 moving window.
(b) Texture features images are scaled to 8-bit.
(c) Signatures of the eight rock units are generated based on training areas for raw Landsat TM, SIR-C and Radarsat images, texture feature images, and various combinations of spectral and textual images.

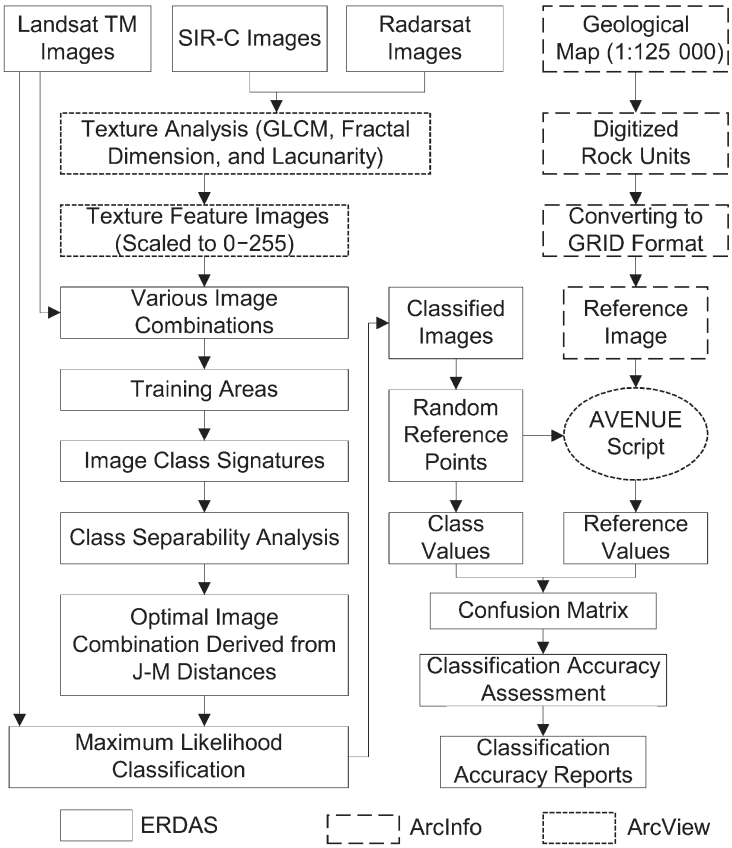

Figure 2. Flow chart of textural feature extraction and spectral/textural image classification.

(d) Class separability analysis is achieved through calculating the Jeffries-Matusita (J-M) distance, and selection of the optimal image combination based on the maximum value of the minimum J-M distances. The J-M distance is a measure of the average distance between the two class density functions. It can be defined as (Richards 1994):

$$d = 2\left(1 - e^{-\beta}\right) \tag{1}$$

where d is the J-M distance, and β is the Bhattacharyya distance between two classes. The calculation of β can be found in Richards (1994). For eight rock unit classes, there are 28 possible class pair combinations, and therefore 28 J-M distance values. The minimum of the 28 values in the range 0–2 is used for comparison between different image combinations. Larger values of the minimum J-M distance mean that class signatures are more separable than those with smaller minimum J-M distance values. The image combination that has the largest minimum J-M distance value is selected as the optimal image combination for classification.

(e) Maximum likelihood classification of the 6-band (exclusive of the thermal band) Landsat TM imagery and the optimal image combination into eight rock unit categories, namely basalt, breccia, clastic, granitic, metasedimentary, Quaternary, schist and volcanic. Metasedimentary rocks and Quaternary

deposits were not included in the first image group (sample images), but were included in the second image group because Landsat TM images were used for classification.

(f) Classified images are obtained for the Landsat TM images and the optimal image combination.

(g) Generation of random sampling point files: Identification numbers and (x, y) coordinates of the random sampling points are stored as text files which will

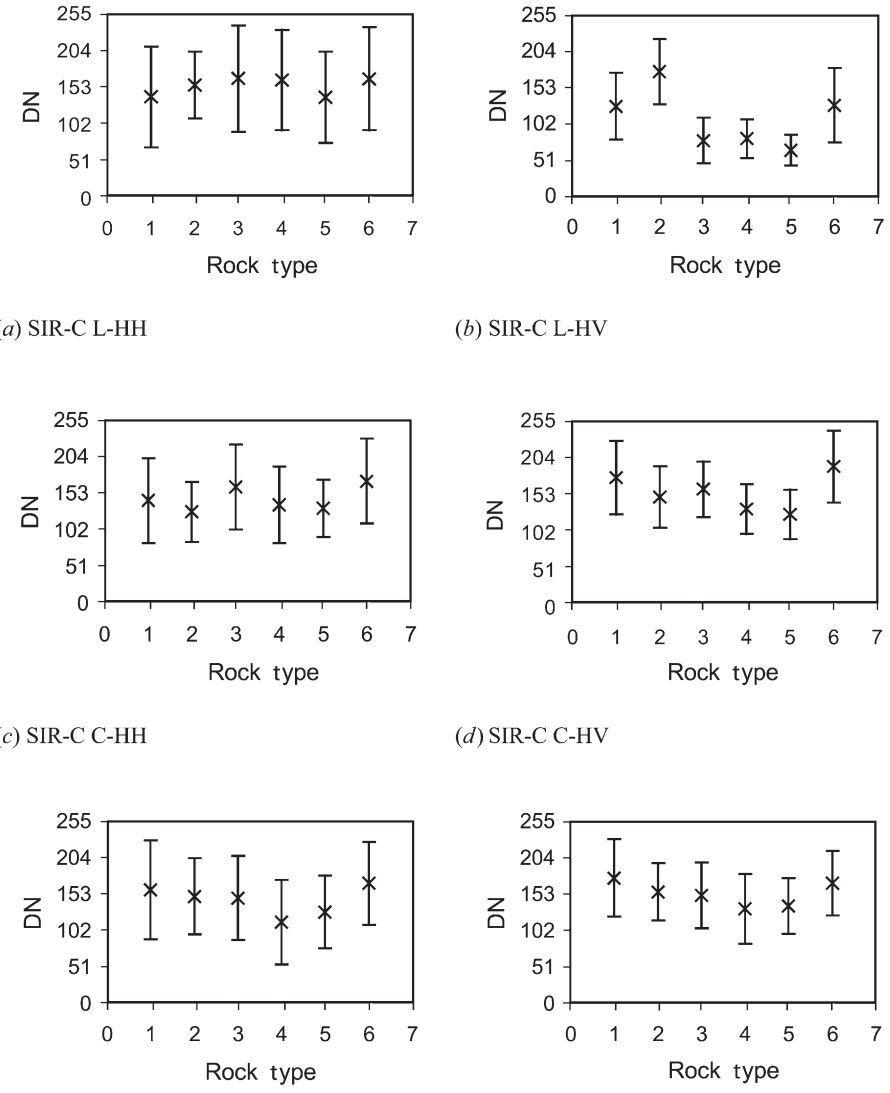

(*a*) SIR-C L-HH (*b*) SIR-C L-HV

(*c*) SIR-C C-HH (*d*) SIR-C C-HV

(*e*) Radarsat STDD4 (*f*) Radarsat EXTH3

Figure 3. Charts showing the mean and the standard deviation around the mean values of digital numbers (DN) in the SIR-C and Radarsat sample images. x = mean, − = standard deviation. 1, breccia; 2, basalt; 3, schist; 4, volcanic; 5, clastic; 6, granitic.

be processed by an ArcView GIS (ESRI) AVENUE script developed in this study to retrieve the rock type of each sampling point.

(h) Rock unit boundaries are digitized from the 1 : 125 000 geological map. Polygon topology is created and attributes are added to each polygon. The digitized rock unit map is then converted into ESRI GRID format.

(i) The ArcView GIS (ESRI) AVENUE script is employed to process the random sampling point files with reference to the GRID format rock unit map. The rock type value for each sampling point is retrieved automatically. Confusion matrices are generated based on class values on the classified images and referenced values on the reference image.

(j) Assessment of classification accuracies: Taking into account the error of omission and error of commission, the classification accuracy for class X can be calculated as the number of correct pixels for class X divided by the sum of the number of correct pixels for class X, the number of omission pixels for class X, and the number of the commission pixels for class X. The classification was conducted on an ERDAS IMAGINE software (ERDAS Inc.), and the accuracy assessment was based on 1024 random sampling points.

4. Results and discussions

4.1. *Sample images*

By comparing the mean DN values and standard deviation bars for the rock sample images extracted from the SIR-C and Radarsat images (figure 3), it appears that the L-HV image shows the most tonal differences of the six rock units. For example, it would be difficult to differentiate breccia and clastic rocks based on their mean DN values in the SIR-C L-HH image, but the two rock units can be well separated from each other in the SIR-C L-HV image.

Figure 4 shows the GLCM-based texture measures (homogeneity, contrast, dissimilarity and entropy) for the sample images. As can be seen, the curves in figure 4 are all relatively flat, which means that the GLCM texture measures may not effectively discriminate different textures of the sample images.

For the differential box counting method (Sarkar and Chaudhuri 1992), fractal dimension values may change with different maximum box sizes used for least-square fitting. Lacunarity is a scale-dependent measure (Gefen *et al.* 1983), and will change with gliding-box size. The fractal dimension as a function of the maximum box size, and the Voss lacunarity and new lacunarity as a function of gliding-box size are shown in figure 5, figure 6 and figure 7, respectively.

From figure 5 it can be seen that basalt generally has higher fractal dimension values than other rock units, particularly on the SIR-C L-HV image (figure 5(*b*)). However, it is difficult to generalize a changing pattern of the fractal dimensions of different rock units, except that the shape of the fractal dimension curves changes with the maximum box size in a similar manner. Comparison between figure 6 and figure 7 indicates that Voss lacunarity generally cannot reveal differences in rock unit textures, particularly at larger gliding-box sizes ($r > 3$). This is in accord with the results in Dong (2000b), and can be attributed to the better approximation of the new lacunarity method (Dong 2000b) to the image intensity surface. As can be seen, the basalt and clastic rocks, which were not differentiable in figure 3, can be well differentiated from each other due to the clear differences in their new lacunarity values on both the SIR-C L-HH image (figure 7(*a*)) and the SIR-C C-HH image (figure 7(*c*)), while such clear differences do not exist in the fractal dimension

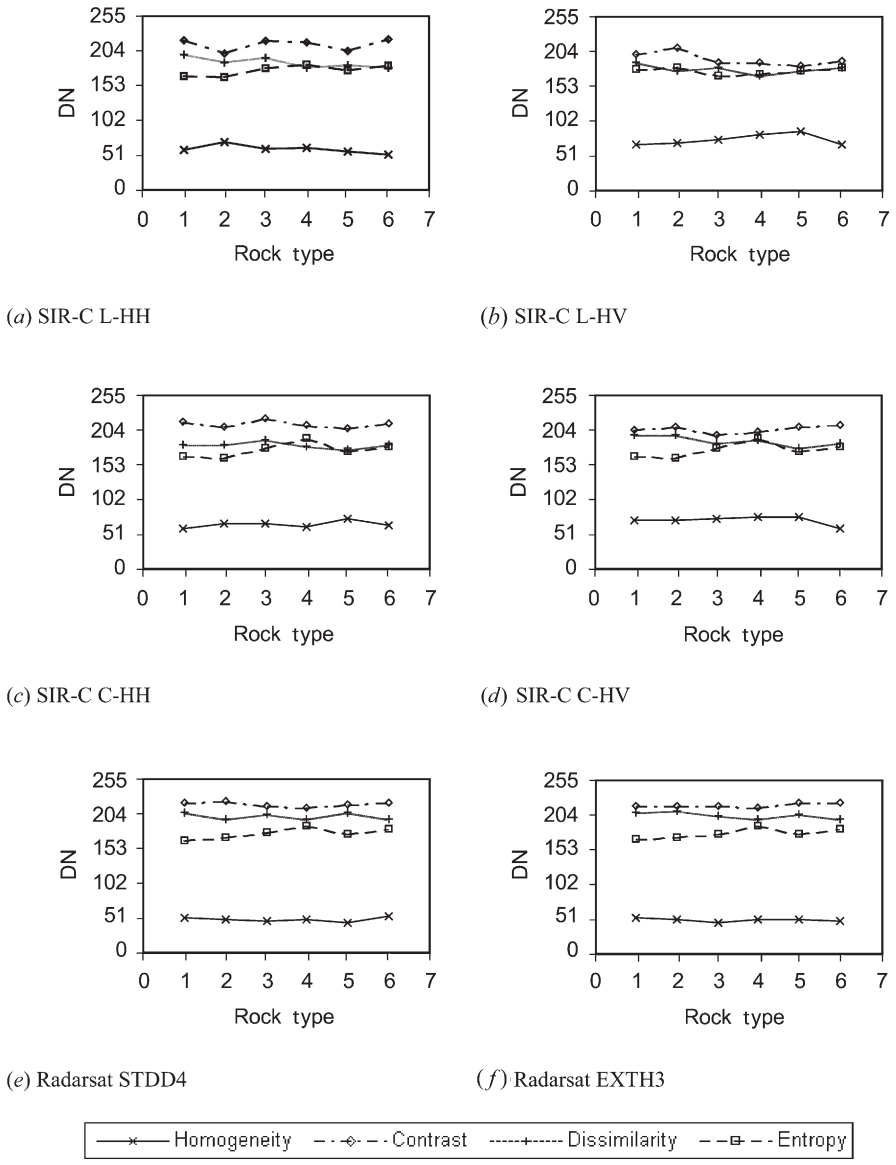

Figure 4. Grey-level co-occurrence matrix (GLCM) texture measures obtained from the sample images. Spatial relationship = (0,1) (i.e. GLCM is constructed based on two adjacent pixels in vertical direction). Texture feature values are scaled into 0–255 for comparison. 1, breccia; 2, basalt; 3, schist; 4, volcanic; 5, clastic; 6, granitic.

curves (figure 4(*a*) and (*c*)) and Voss lacunarity curves (figure 5(*a*) and (*c*)) of the same images. Table 3 lists the comparison of five different rock unit pairs based on their fractal dimension and lacunarity curves shown in figure 5 and figure 7. In general, the new grey-scale lacunarity measure is better than fractal dimension and Voss lacunarity in discriminating different image textures of rock types in this study. As far as image type is concerned, the SIR-C L-HH image is better than other SIR-C images and Radarsat images for discrimination of rock unit textures,

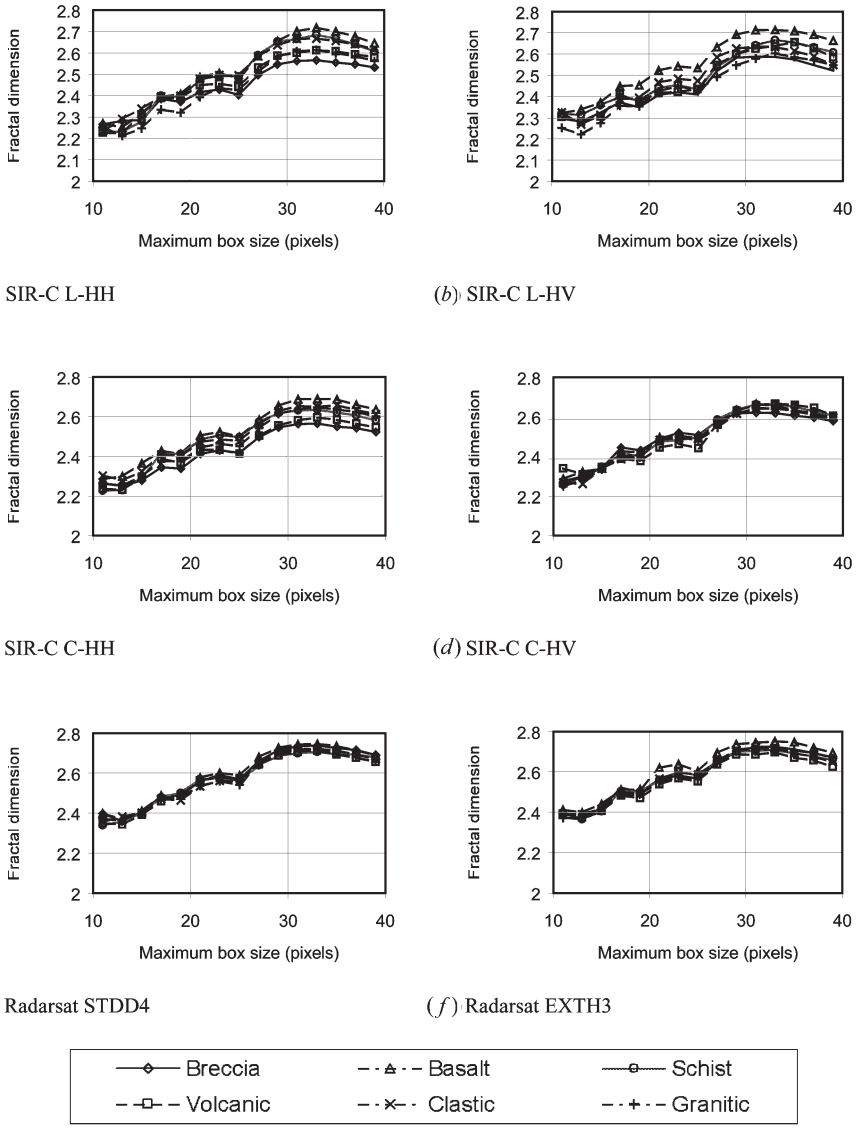

Figure 5. Fractal dimension as a function of maximum box size for selected rock unit sample images. The fractal dimension values are obtained using the differential box counting method proposed by Sarkar and Chaudhuri (1992).

and co-polarization (HH) generally provides more textural information than cross-polarization (HV) in the study area.

Figure 3 shows that the L-HV image may be more useful for discriminating different rock units than the L-HH image as far as image tone is concerned. In fact, many theories believe that cross-polarized return is dominated by subsurface volume scattering (Blanchard and Rouse 1980, Fung and Eom 1981), and that the relative cross-polarized return is much lower than like-polarized (Fung and Ulaby 1983). Schaber *et al.* (1997) believe that the improved discrimination of rock unit tones in cross-polarized images is mainly a result of increased backscattering

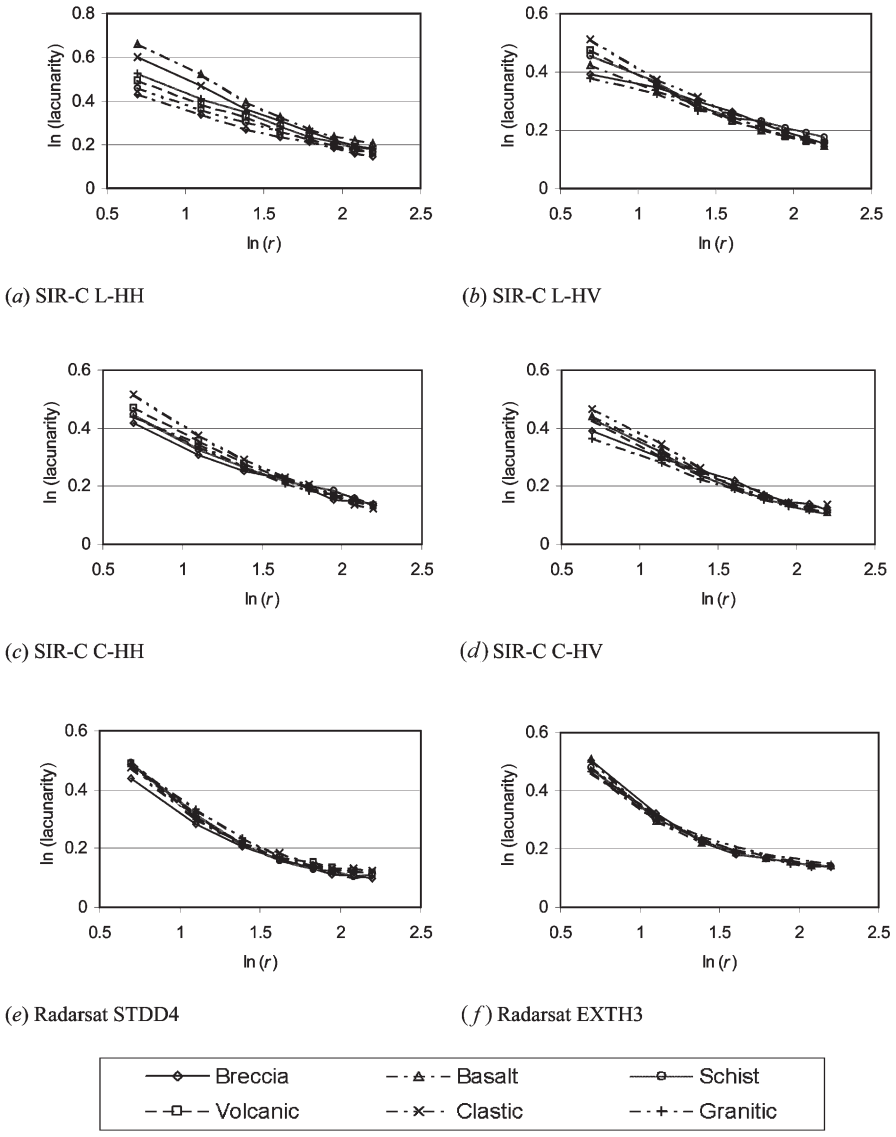

Figure 6. Voss lacunarity as a function of gliding-box size for selected rock unit sample images. The lacunarity values are calculated using the estimation method proposed by Voss (1986), with gliding-box size $r = 2$, 3, 4, 5, 6, 7, 8 and 9.

contrast of rock units. In the study area, for example, the basalt unit can be easily identified on the L-HV image by its bright tones. Since the study area has no vegetation cover, the relatively high cross-polarized (HV) return from the basalt flow unit cannot be related to vegetation canopies, which are strong volume scatterers due to multiple reflection of branches and twigs (National Aeronautics and Space Administration (NASA) 1989). The study area is in an extremely arid environment, and the fine-grained vesicular basalt flows form prominent black mesas with large sub-rounded boulders (Morton 1977). Therefore, the relatively high HV return from the basalt unit can be attributed to multiple scattering from

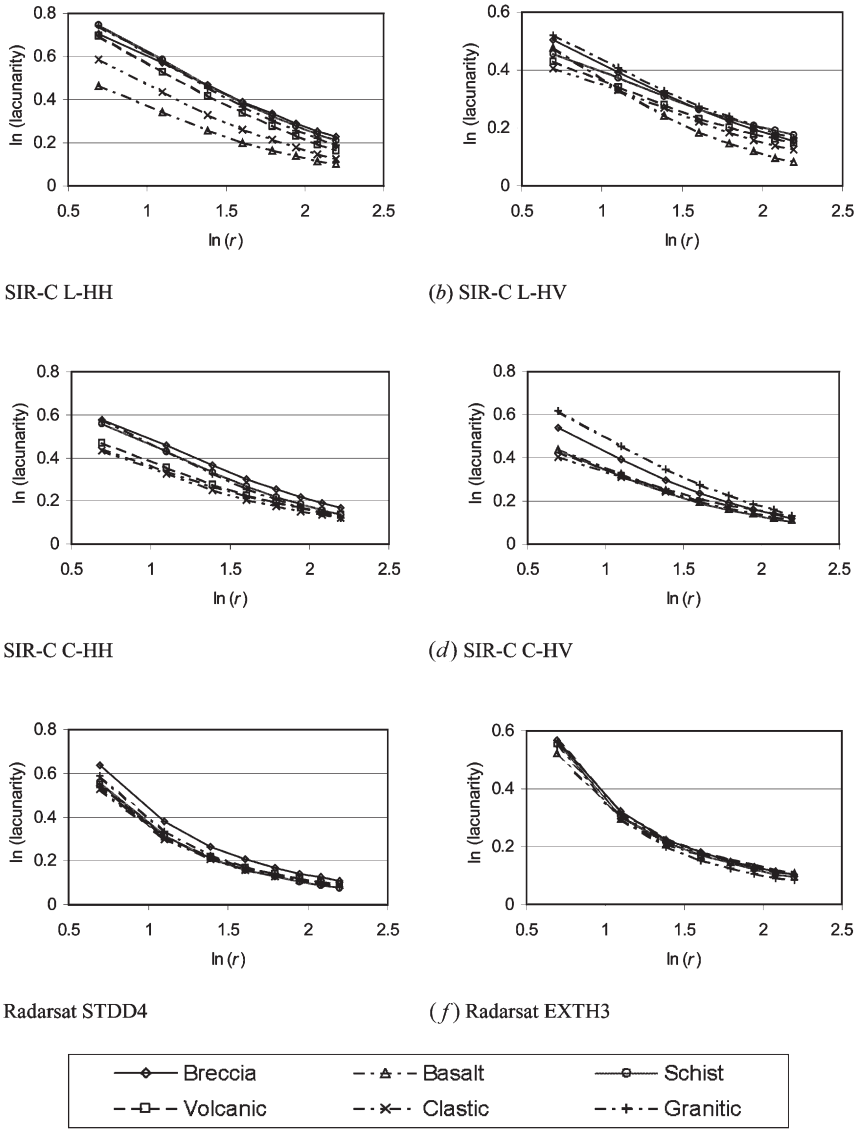

Figure 7. Non-directional lacunarity as a function of gliding-box size for selected rock unit sample images. The lacunarity values are calculated using the new estimation method proposed by Dong (2000b), with gliding-box size $r = 2, 3, 4, 5, 6, 7, 8$ and 9.

the extremely rough surface of the unit. However, cross-polarization may not be better than co-polarization when textural information of the image is under study, as shown in the results from fractal dimension and lacunarity measurements.

The new lacunarity measurements (figure 7) seem to have geological significance which is not obvious in the Voss lacunarity results (figure 6). For the new lacunarity curves of the SIR-C images (figure 6(*a*)–(*d*)), breccia, schist and granitic rocks generally have higher lacunarity, while basalt and clastic rocks have lower lacunarity, and volcanic rocks have lacunarity values between 'high' and 'low'. Such a pattern seems to be related to the weathering resistance of the rocks. In fact,

Table 3. Comparison of five rock unit pairs based on their fractal dimension and new lacunarity curves.*

	Pair 1		Pair 2		Pair 3		Pair 4		Pair 5	
	L	F	L	F	L	F	L	F	L	F
L-HH	v	x	v	x	v	o	v	o	x	x
L-HV	o	o	o	o	o	o	o	o	o	x
C-HH	o	x	x	o	o	o	o	o	o	x
C-HV	x	x	x	x	x	x	o	x	o	x
STDD4	x	x	x	x	x	x	o	x	x	x
EXTH3	x	x	x	x	x	x	x	x	x	x

*Pair 1, breccia and clastic; pair 2, basalt and schist; pair 3, basalt and volcanic; pair 4, breccia and basalt; pair 5, volcanic and granitic. F, fractal dimension; L, lacunarity; v, well separated; o, moderately separated; x, not separated.

many mountain ridges are composed of highly resistant rocks. The ridge slopes can create strong backscatter under certain radar illumination conditions. For the Radarsat STDD4 and EXTH3 images, both fractal dimension and lacunarity curves fail to show the differences of rock unit image textures, except that the lacunarity curves for Radarsat STDD4 (figure 7(*e*)) show that breccia has higher lacunarity than other rock units. Visual examination of the Radarsat STDD4 and EXTH3 sample images for breccia indicates that the ridges have brighter tones on the STDD4 image than on the EXTH3 image, which can be explained by the lower incidence angle of STDD4 than EXTH3 (see table 2). With a higher incidence angle, the EXTH3 image reduces the layover effects that appear on the STDD4 image as brighter belts. The results from the lacunarity curves of the SIR-C and sample images suggest that images with a 'coarser' texture (sharp contrast between bright and dark) generally have higher lacunarity than images with a 'smoother' texture (less contrast between bright and dark). It should be noted that high lacunarity values at a certain scale do not necessarily mean that different texture patterns can be better discriminated at that scale than at other scales, because the discrimination of textures depends on the differences in their lacunarity measurements instead of absolute lacunarity values. This has been shown in Dong (2000a), where Brodatz textures can be better discriminated at scale $r=5$ than at $r=2$, 3, 4, 6 or 7. Also, it would be difficult to conclude in general which scale provides the best discrimination ability, as the lacunarity measure is scene-dependent. More importantly, since lacunarity is scale-dependent, the use of lacunarity measure at a single scale would be limited compared with the lacunarity measures at different scales.

4.2. *Full scenes*

With six Landsat TM bands, four SIR-C images, two Radarsat images, and various textural feature images from the radar images, the image combinations for classification can be numerous. To select the optimal image combination for rock unit discrimination using spectral and textural information, the J-M distances are calculated for: (1) individual and combined Landsat TM bands; (2) individual and combined SIR-C images; (3) combined Landsat TM and SIR-C textural feature images; and (4) combined Landsat TM and Radarsat textural feature images. Since the results from sample images show that the SIR-C L-HH image is better than

other images for textural analysis, full scene textural feature images are obtained mainly from the SIR-C L-HH image. To reduce the number of possible image combinations, non-directional lacunarity and lacunarity in 135° direction are taken into account, and not all directions are calculated. Figure 8 lists the image bands or image combinations that have a minimum J-M distance greater than 0.01. The J-M distances resulted from individual SIR-C images and their lacunarity images are generally very small (< 0.01, not shown in figure 8, except for the L-HH lacunarity image). From the image combinations 4, 5, 7, 8 and 9 in figure 8, it can be seen that Landsat TM data contained more separable rock unit information than did the combination of SIR-C images and the lacunarity images of the SIR-C L-HH image. The J-M distance values show that the new lacunarity measures outperformed the Voss lacunarity, the fractal dimension, and the GLCM texture measures, which has

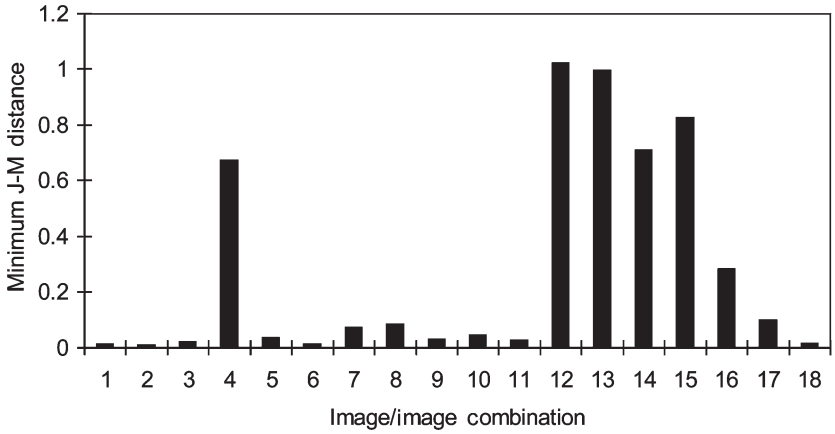

Image/image combinations:
1. Landsat TM band 2
2. Landsat TM band 3
3. Landsat TM band 7
4. Landsat TM all bands
5. SIR-C L-HH, L-HV, C-HH, and C-HV
6. SIR-C L-HH new lacunarity image at r =3
7. SIR-C L-HH new lacunarity images at r = 3, 5, 7, non-directional
8. SIR-C L-HH new lacunarity images at r = 3, 5, 7, θ = 135°
9. SIR-C L-HH Voss lacunarity images at r = 3, 5, 7
10. SIR-C L-HH GLCM textural images*
11. SIR-C C-HH GLCM textural images*
12. TM all bands, SIR-C L-HH new lacunarity images at r = 3, 5, 7, θ = 135°
13. TM all bands, SIR-C L-HH new lacunarity images at r = 3, 5, 7, non-directional
14. TM all bands, SIR-C L-HH fractal dimension image
15. TM all bands, SIR-C L-HH GLCM textural images*
16. TM all bands, Radarsat lacunarity images at r = 3, 5, 7, θ = 135°
17. SIR-C all bands, SIR-C L-HH new lacunarity images at r = 3, 5, 7, θ = 135°
18. SIR-C all bands, SIR-C L-HH GLCM textural images*

* GLCM textural measures include homogeneity, dissimilarity, contrast and entropy.

Figure 8. Separability of classes (minimum J-M distance) from different images and image combinations. Results from lacunarity images of SIR-C L-HV, C-HH, C-HV and Radarsat images are not shown due to the small J-M distance values (< 0.01).

also been shown in a previous paper using Brodatz textures (Dong 2000b). The image combinations 5–11 in figure 8 show that the SIR-C L-HH image generally contains more textural information of the rock units than L-HV, C-HH and C-HV images (J-M distances from lacunarity images of L-HV, C-HH and C-HV are less than 0.01 and are not shown in figure 8). Image combinations 10 and 11 seem to indicate that L-band is better than C-band for differentiating rock unit textures. As can be seen in the J-M distance values (figure 8), the combination of TM all bands and SIR-C L-HH new lacunarity images at $r=3$, 5, 7, $\theta=135^\circ$ is the optimal combination for rock unit classification, and SIR-C images generally provide more textural information than Radarsat images in the study area. The optimal combination is used for classification.

From table 4, it can be seen that the classification accuracy is relatively low for both the Landsat TM six bands (bands 1, 2, 3, 4, 5 and 7), and the optimal image combination, but the classification accuracy increased 8.31% on average, from an average of 25.35% for the TM bands to an average of 33.65% for the optimal image combination.

In a previous publication (Dong 2000b), it has been shown with Brodatz textures that lacunarity measures can reveal the scaling properties of textures: a texture X can be discriminated from texture Y at certain scales (or gliding-box sizes), while X and Y may not be differentiated at some other scales. As an example, figure 9 shows the SIR-C L-HH image of the whole study area (25 km × 15 km) and its lacunarity images with the gliding-box size $r=3$, 5 and 7, and the direction of lacunarity being 135°. Visual inspection can tell that the lacunarity images at different scales (gliding-box sizes) are different. For example, a breccia unit can be seen as bright tones in the central part of the left-half image when $r=3$ (figure 9(*b*)). This bright-tone unit gradually becomes invisible when $r=5$ (figure 9(*c*)) and $r=7$ (figure 9(*d*)). Such scaling properties of rock unit textures may be important factors for increasing image classification accuracy due to the complementary nature of lacunarity images at different scales. In addition, figure 9 can be related to figure 7(*a*), which is based on sample images of size 79 × 79 pixels (987.5 m × 987.5 m on the ground). For example, basalt and clastic rocks generally have lower DN values, while schist and breccia have higher DN values on the lacunarity images, as displayed in the lacunarity curves (figure 7(*a*)).

The results from the fractal dimension and lacunarity curves and class

Table 4. Comparison of classification accuracy values for Landsat TM six bands and the optimal TM and SIR-C L-HH directional lacunarity image combination as shown in figure 8.

	Classification accuracy (%)	
Class	Landsat TM six bands	TM and SIR-C L-HH lacunarity images
Quaternary	23.51	28.08
Basalt	47.64	62.21
Breccia	17.78	28.13
Clastic	25.09	39.37
Granitic	16.87	20.65
Schist	21.24	29.73
Volcanic	36.12	44.09
Metasedimentary	14.58	17.00
Average Accuracy	25.35	33.66

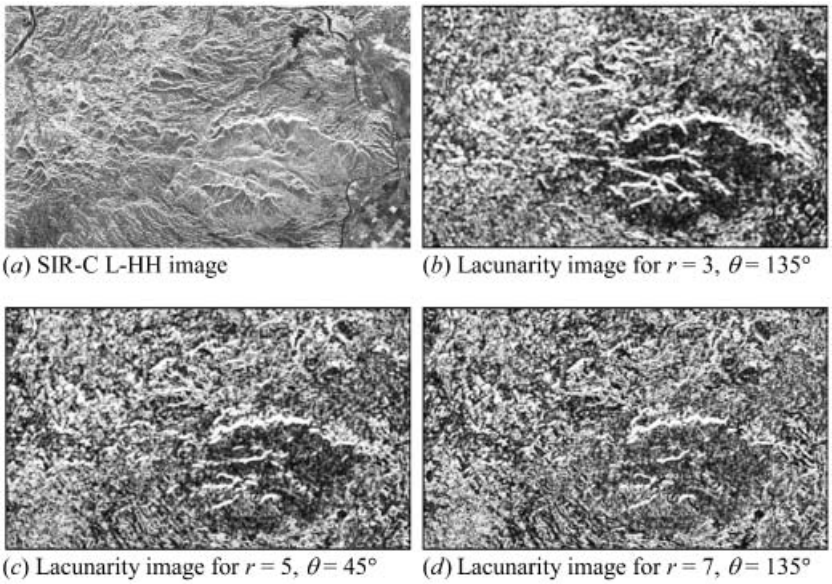

Figure 9. SIR-C L-band HH polarization image and its directional lacunarity images. r, gliding-box size; θ, direction of lacunarity measurement.

separability measures (J-M distance) indicate that the SIR-C L-HH image is more suited for textural analysis of rock units than other SIR-C images and Radarsat images, and that co-polarization (HH) generally provides more textural information than cross-polarization (HV) in the study area, which might also be true for other areas with similar environments. It should be noted that this conclusion is referred to the textural content of the SIR-C images, rather than image spectral dimension. Indeed, statistical results based on image spectral dimension (figure 3) do show that the L-HV image is better than other radar images for rock unit discrimination in the study area, which also supports the conclusions by Evans *et al*. (1986) and Schaber *et al*. (1997). However, as far as texture is concerned, the relatively strong HH polarization return of topographic slopes help enhance the texture expression of rock units.

Compared with the C-band HH polarization SIR-C image, the C-band HH polarization Radarsat images of both the STDD4 and the EXTH3 have poorer performance in revealing textural information of the rock units in the study area. This can be partly attributed to three factors.

1. *Radar incidence angle*. Singhroy and Saint-Jean (1999) analysed the relief effects of Radarsat incidence angles in a part of Cape Breton Highlands, Canada, and concluded that steeper incidence angles (20–27°) are more suitable for delineating structural and geomorphic features than shallow incidence angles (45–49°), which is partly in accord with our results that the incidence angle (23°) of SIR-C is more effective in revealing rock unit textures than the lower incidence angle Radarsat images in the study area.

2. *Radar look direction*. There is an approximately 45° difference between the SIR-C look direction and the Radarsat look direction due to the difference between the Shuttle Endeavor flight path and the Radarsat orbit. The general trend of the topographic slopes in the study area is in the NW–SE direction which is nearly

perpendicular to the SIR-C radar look directions. Therefore, the major topographic slopes are more enhanced on the SIR-C images than on Radarsat images, which may affect the image texture expression of the rock units.

3. *Image resampling effects*. Roy and Dikshit (1994) concluded that image resampling may modify the image texture in a complex manner when the image does not have a homogeneous grey-level structure. In this study, no resampling was conducted for the SIR-C images, while Radarsat images were resampled using cubic interpolation during the process of registration with the SIR-C images. It is possible that resampling process degraded the textural expression of the Radarsat images.

It is believed that the improved classification accuracy from combined Landsat TM and lacunarity feature images from the SIR-C L-HH image, as compared to Landsat TM images, can be mainly attributed to the complementary nature of lacunarity images on different scales, as shown in figure 9, just like multiple spectral bands can be combined to obtain better classification results when the bands are poorly correlated. This conclusion is based on three facts: (a) previous studies on Brodatz textures have shown that lacunarity measures on different scales and in different directions can improve classification accuracy (Dong 2000a, b); (b) class separability results (J-M distances) show that the lacunarity image of the L-HH image can be better than that of the other SIR-C images for rock unit discrimination; and (c) the optimal image combination includes lacunarity images of the L-HH image instead of the raw L-HH image, therefore the contribution of the L-HH image in the classification is mainly from the textural components of the image, rather than from the raw L-HH image as an ancillary band.

The relatively low classification accuracy for both the Landsat TM six bands (bands 1, 2, 3, 4, 5 and 7) and the optimal image combination can be attributed to the following factors.

(1) The geological map used as reference is stratigraphic rather than lithologic. It shows rock units identified by age rather than rock type. It is possible that rock units with different ages may have similar spectral responses in Landsat TM images because similar rock compositions may appear in different stratigraphic units. For radar images, the backscatter responses are related to radar system parameters and target parameters such as dielectric constant, surface roughness and volume scattering (Fung and Ulaby 1983). For terrestrial rocks in an arid environment, the density of a rock is the major factor affecting the dielectric constant, but the dielectric constant variations do not have substantial influence on radar signal because most natural rocks have dielectric constants in a narrow range (Farr 1993). These parameters generally have no direct link to the age of the rock units, even though they may reflect the age of the rock units in some cases.
(2) The geological map used as reference is for bedrock geology, not for surficial geology. During field investigation, a geologist often makes logical deductions as to the rock type buried under layers of unconsolidated Quaternary deposits. These unconsolidated deposits were treated as invisible when the geologist makes the map. The unconsolidated deposits are generally not invisible to an electro-optical sensor like Landsat TM, but can be invisible to radar imaging systems due to the penetration ability of radar waves under certain conditions.
(3) Contrary to (2), the geologist may have mapped a rock unit in a certain

area, but the distribution area of the rock unit in Landsat TM and radar images can be larger than on the map because of the similarity in the spectral responses of the rock unit and its weathering products, and possible penetration abilities of radar waves through thin layers of unconsolidated Quaternary deposits. In our study, for example, the lava flows form an ε-shaped unit on the geological map, but the TM and radar images all show that the shape of the units is close to an ellipse.

(4) As shown in the class separability results (figure 8), Landsat TM data contained much more separable rock unit information than did the lacunarity images of the SIR-C L-HH image, which means that the classification accuracy of the TM and SIR-C L-HH lacunarity images combination mainly depends on the contribution of the Landsat TM images, even though the incorporation of SIR-C L-HH lacunarity images can improve the classification accuracy. In other words, if the classification accuracy from the Landsat TM images is relatively low, the classification accuracy of the Landsat TM and SIR-C L-HH lacunarity images combination will not be very high.

5. Conclusions

The results of this study suggest that: (1) the SIR-C L-HH image is more suited for textural analysis of rock units than other SIR-C images and Radarsat images, and that co-polarization (HH) generally provides more textural information than cross-polarization (HV) in the study area; (2) the new grey-scale lacunarity measures from radar images can reveal more textural information for rock unit discrimination than other textural measures, and combination of spectral information from Landsat TM images and textural information obtained through lacunarity measurement of radar images can improve the classification accuracy of rock units; and (3) the scaling properties of rock unit textures on radar images can be revealed by lacunarity measures. The results from Radarsat STDD4 and EXTH3 are not satisfactory for rock unit discrimination in this area. It would be useful to test other Radarsat imaging modes due to the fact that radar incidence angle may affect radar image texture. While SIR-C L-HH image outperformed other radar images for texture analysis of rock units in the study area, SIR-C L-HV image is more useful for discriminating different rock units than the L-HH image based on image DN values. It would be interesting to compare multi-polarization SIR-C images with images from Radarsat-II which is scheduled for launch in 2005 with C-band horizontal (HH), vertical (VV) and cross (HV and VH) polarizations. However, pixel-by-pixel classification of multi-polarization radar images may not be very useful in the study area, as indicated by the class separability analysis results from the dual-band (L and C) and dual-polarization (HH and HV) SIR-C images. Due to the lack of L-band, Radarsat-II images may not be better than SIR-C L-HH images in revealing textures of rock units in similar environments. In the past years, wavelets have been used as a multi-scale analysis method that separates information of different scales (Mallat 1989, Ranchin and Wald 1993, Wornell 1995). It would be useful to combine lacunarity with other measures such as wavelet for better understanding of the scaling properties of rock unit textures. The study area is in an arid environment with relatively clear rock exposure and no vegetation cover, which greatly eliminates the influence of soil moisture and vegetation on radar signals. It is expected that lacunarity analysis, as a general approach to textural measurement, can be used in a different environment to aid in rock unit

discrimination as well as other land-cover applications. However, the effectiveness may vary with the environment because rock unit texture and image signals can be heavily affected by weathering conditions, vegetation cover and other factors.

Acknowledgments

The authors would like to thank Dr Paul F. Williams for his support in this study. We would also like to thank the USGS EROS Data Center for providing the Shuttle Imaging Radar (SIR-C) data, and the Canada Centre for Remote Sensing (CCRS) for providing Landsat TM and Radarsat data to P. Dong (principal investigator) through the Earth Observation Data Sets (EODS) program.

References

ALLAIN, C., and CLOITRE, M., 1991, Characterizing the lacunarity of random and deterministic fractal set. *Physical Review A*, **44**, 3552–3558.

ANYS, H., BANNARI, A., HE, D. C., and MORIN, D., 1994, Texture analysis for the mapping of urban areas using airborne MEIS-II images. *First International Airborne Remote Sensing Conference and Exhibition, Strasbourg, France, 11–15 September, 1994* (Ann Arbor, MI: ERIM), pp. 622–629.

ARAI, K., 1993, A classification method with a spatial-spectral variability. *International Journal of Remote Sensing*, **14**, 699–709.

BERBEROGLU, S., LLOYD, C. D., ATKINSON, P. M., and CURRAN, P. J., 2000, The integration of spectral and textural information using neural networks for land cover mapping in the Mediterranean. *Computers and Geosciences*, **26**, 385–396.

BLANCHARD, A. J., and ROUSE, J. W., 1980, Depolarization of electromagnetic waves scattered from an inhomogeneous half space bounded by a rough surface. *Radio Science*, **15**, 773–779.

BLOM, R. G., and DAILY, M., 1982, Radar image processing for rock-type discrimination. *IEEE Transactions on Geoscience and Remote Sensing*, **20**, 343–351.

BRODATZ, P., 1966, *Texture: A Photographic Album for Artists and Designers* (New York: Dover).

CHICA-OLMO, M., and ABARCA-HERNAÂNDEZ, F., 2000, Computing geostatistical image texture for remotely sensed data classification. *Computers and Geosciences*, **26**, 373–383.

DELLEPIANE, S., GIUSTO, D. D., SERPICO, S. B., and VERNAZZA, G., 1991, SAR image recognition by integration of intensity and textural information. *International Journal of Remote Sensing*, **12**, 1915–1932.

DESJARDINS, L., 1950, Techniques in photogeology. *Bulletin of the American Association of Petroleum Geologists*, **34**, December.

DONG, P., 2000a, Lacunarity for spatial heterogeneity measurement in GIS. *Geographical Information Sciences*, **6**, 1–7.

DONG, P., 2000b, Test of a new lacunarity estimation method for image texture analysis. *International Journal of Remote Sensing*, **21**, 3369–3373.

DURAND, J. M., GIMONET, B. J., and PERBOS, J. R., 1987, SAR data filtering for classification. *IEEE Transactions on Geoscience and Remote Sensing*, **25**, 629–637.

ELACHI, C., 1982, Radar images from space. *Scientific American*, **247**, 54–61.

EVANS, D., 1988, Multisensor classification of sedimentary rocks. *Remote Sensing of Environment*, **25**, 129–144.

EVANS, D. L., FAR, T. G., FORD, J. P., THOMPSON, T. W., and WERNER, C. L., 1986, Multipolarization radar images for geologic mapping and vegetation discrimination. *IEEE Transactions on Geoscience and Remote Sensing*, **24**, 246–257.

FARR, T., 1993, Guide to Magellan image interpretation (chapter 5). JPL Publication 93-24, National Aeronautics and Space Administration.

FRANKLIN, S. E., and PEDDLE, D. R., 1989, Spectral texture for improving class discrimination in complex terrain. *International Journal of Remote Sensing*, **10**, 1437–1443.

FRANKLIN, S. E., and PEDDLE, D. R., 1990, Classification of SPOT HRV imagery and texture features. *International Journal of Remote Sensing*, **11**, 551–556.

FUNG, A. K., and EOM, H. J., 1981, Note on the Kirchoff rough surface solution in backscattering. *Radio Science*, **16**, 299–302.

FUNG, A. K., and ULABY, F. T., 1983, Matter–energy interaction in the microwave region. In *Manual of Remote Sensing*, 2nd edn, vol. 1, edited by R. N. Colwell (Falls Church, USA: Sheridan Press and American Society of Photogrammetry), pp. 115–164.

GADDIS, L., MOUGINIS-MARK, P., SINGER, R., and KAUPP, V., 1989, Geologic analysis of Shuttle Imaging Radar (SIR-B) data of Kilauea Volcano, Hawaii. *Geological Society of America Bulletin*, **101**, 317–332.

GADDIS, L., MOUGINIS-MARK, P. J., and HAYASHI, J. N., 1990, Lava flow surface texture: SIR-B radar image texture, field observations, and terrain measurements. *Photogrammetric Engineering and Remote Sensing*, **56**, 211–224.

GEFEN, Y., MEIR, Y., and AHARONY, A., 1983, Geometric implementation of hypercubic lattices with noninteger dimensionality by use of low lacunarity fractal lattices. *Physical Review Letters*, **50**, 145–148.

GONG, P., MARCEAU, D. J., and HOWARTH, P. J., 1992, A comparison of spatial feature extraction algorithms for land-use classification with SPOT HRV data. *Remote Sensing of Environment*, **40**, 137–151.

GREENBAUM, D., 1987, Lithological discrimination of central Snowdonia using airborne multispectral scanner imagery. *International Journal of Remote Sensing*, **8**, 799–816.

HARALICK, R. M., and SHANMUGAM, K., 1974, Combined spectral and spatial processing of ERTS imagery. *Remote Sensing of Environment*, **3**, 3–13.

HARALICK, R. M., SHANMUGAM, K., and DINSTEIN, I., 1973, Texture features for image classification. *IEEE Transactions on Systems, Man and Cybernetics*, **3**, 610–621.

HENEBRY, G. M., and KUX, H. J. H., 1995, Lacunarity as a texture measure for SAR imagery. *International Journal of Remote Sensing*, **16**, 565–571.

HENEBRY, G. M., and KUX, H. J. H., 1996, Spatio-temporal land cover dynamics in the Pantanal assessed using lacunarity analysis on an ERS-1 SAR image time series. *Proceedings of IGARSS '96, Lincoln, Nebraska, 27–31 May 1996* (Lincoln, NE: IEEE), pp. 195–197.

KAHLE, A. B., and GOETZ, A. F. H., 1983, Mineralogic information from a new airborne thermal infrared multispectral scanner. *Science*, New York, **222**, 24–27.

KURVONEN, L., and HALLIKAINEN, M. T., 1999, Textural information of multitemporal ERS-1 and JERS-1 SAR images with applications to land and forest type classification in boreal zone. *IEEE Transactions on Geoscience and Remote Sensing*, **37**, 680–689.

KUX, H. J. H., and HENEBRY, G. M., 1994a, Multi-scale texture in SAR imagery: landscape dynamics of the Pantanal, Brazil. *Proceedings of IGARSS '94, Pasadena, California, 8–14 August 1994* (Pasadena, CA: California Institute of Technology), pp. 1359–1364.

KUX, H. J. H., and HENEBRY, G. M., 1994b, Evaluating anisotropy in SAR imagery using lacunarity functions. *International Archives of Photogrammetry and Remote Sensing*, **30**, 141–145.

MALLAT, S., 1989, A theory for multiresolution signal decomposition: the wavelet representation. *IEEE Transactions on Pattern Analysis and Machine Intelligence*, **11**, 674–693.

MANDELBROT, B. B., 1977, *Fractals, Forms, Chance and Dimension* (San Francisco, CA: Freeman).

MANDELBROT, B. B., 1982, *The Fractal Geometry of Nature* (San Francisco, CA: Freeman).

MARCEAU, D. J., HOWARTH, P. J., DUBOIS, J. M. M., and GRATTON, D. J., 1990, Evaluation of the grey-level cooccurrence matrix method for land-cover classification using SPOT imagery. *IEEE Transactions on Geoscience and Remote Sensing*, **28**, 513–518.

MATHER, P. M., TSO, B., and KOCH, M., 1998, An evaluation of Landsat TM spectral data and SAR-derived textural information for lithological discrimination in the Red-Sea Hills, Sudan. *International Journal of Remote Sensing*, **19**, 587–604.

MELTON, F. A., 1945, Preliminary observations on geological use of aerial photographs. *Bulletin of American Association of Petroleum Geologists*, **29**, 1756–1765.

MILLER, V. G., 1961, *Photogeology* (New York: McGraw-Hill).

MORTON, P. K., 1966, Geologic map of Imperial County, California. State of California, The Resources Agency (Sacramento, CA: Department of Conservation).

MORTON, P. K., 1977, Geology and mineral resources of Imperial County, California. County Report 7 (Sacramento, CA: California Division of Mines and Geology).

NATIONAL AERONAUTICS AND SPACE ADMINISTRATION (NASA), 1989, SAR—Synthetic Aperture Radar—Instrument panel report. Earth Observation System Reports, Vol. IIf (Pasadena, CA: NASA).

NOWHUYS, J. J. VAN, 1937, Geological interpretation of aerial photographs. *Transactions of American Institute of Mining and Metallurgy Engineers*, **126**, 607–624.

PEDDLE, D. R., and FRANKLIN, S. E., 1991, Image texture processing and data integration for surface pattern discrimination. *Photogrammetric Engineering and Remote Sensing*, **57**, 413–420.

PENTLAND, A., 1984, Fractal-based description of natural scenes. *IEEE Transactions on Pattern Analysis and Machine Intelligence*, **6**, 661–674.

PLOTNICK, R. E., GARDNER, R. H., and O'NEILL, R. V., 1993, Lacunarity indices as measures of landscape texture. *Landscape Ecology*, **8**, 201–211.

PLOTNICK, R. E., GARDNER, R. H., HARGROVE, W. W., PRESTEGAARD, K., and PERLMUTTER, M., 1996, Lacunarity analysis: a general technique for the analysis of spatial patterns. *Physical Review E*, **53**, 5461–5468.

PRIHATNO, K. B., 1995, Forest classification using texture analysis. M.Eng. Report, University of New Brunswick, Canada.

RANCHIN, T., and WALD, L., 1993, The wavelet transform for the analysis of remotely sensed data. *International Journal of Remote Sensing*, **14**, 615–619.

RANSON, K. J., and SUN, G., 1997, An evaluation of AIRSAR and SIR-C/X-SAR images for mapping northern forest attributes in Maine, USA. *Remote Sensing of Environment*, **59**, 203–222.

RICHARDS, J. A., 1994, *Remote Sensing Digital Image Analysis: An Introduction* (Berlin: Springer-Verlag).

RIGNOT, E., and KWOK, R., 1993, Characterization of spatial statistics of distributed targets in SAR data. *International Journal of Remote Sensing*, **14**, 345–363.

ROY, D. P., and DIKSHIT, O., 1994, Investigation of image resampling effects upon the textural information content of a high spatial resolution remotely sensed image. *International Journal of Remote Sensing*, **15**, 1123–1130.

SABINS, F. F. JR, 1987, *Remote Sensing Principles and Interpretation*, 2nd edn (New York: Freeman).

SARKAR, N., and CHAUDHURI, B. B., 1992, An efficient approach to estimate fractal dimension of textural images. *Pattern Recognition*, **25**, 1035–1041.

SCHABER, G. G., MCCAULEY, J. F., and BREED, C. S., 1997, The use of multifrequency and polarimetric SIR-C/X-SAR data in geologic studies of Bir-Safsaf, Egypt. *Remote Sensing of Environment*, **59**, 337–363.

SHANMUGAM, S., NARAYANAN, V., FROST, V. S., STILES, J. A., and HOLTZMAN, J. C., 1981, Textural features for radar image analysis. *IEEE Transactions on Geoscience and Remote Sensing*, **19**, 153–156.

SIMONETT, D. S., and DAVIS, R. E., 1983, Image analysis—active microwave. In *Manual of Remote Sensing*, 2nd edn, vol. 1, edited by R. N. Colwell (Falls Church, USA: The Sheridan Press and American Society of Photogrammetry), pp. 1125–1181.

SINGHROY, V., and SAINT-JEAN, R., 1999, Effects of relief on the selection of Radarsat-1 incidence angle for geological applications. *Canadian Journal of Remote Sensing*, **25**, 211–217.

SMITH, T. G. JR, LANGE, G. D., and MARKS, W. B., 1996, Fractal methods and results in cellular morphology—dimensions, lacunarity and multifractals. *Journal of Neuroscience Methods*, **69**, 123–136.

ULABY, F. T., KOUYATE, F., BRISCO, B., and WILLIAMS, T. H. L., 1986, Textural information in SAR images. *IEEE Transactions on Geoscience and Remote Sensing*, **24**, 235–245.

VANDERMEER, F., 1996, Spectral mixture modeling and spectral stratigraphy in carbonate lithofacies mapping. *ISPRS Journal of Photogrammetry and Remote Sensing*, **51**, 150–162.

VOSS, R., 1986, Random fractals: characterization and measurement. In *Scaling Phenomena in Disordered Systems*, edited by R. Pynn and A. Skjeltorp (New York: Plenum), pp. 37–48.

WANG, L., and HE, D. C., 1990, A new statistical approach for texture analysis. *Photogrammetric Engineering and Remote Sensing*, **56**, 61–66.

WESZKA, J., DYER, C., and ROSENFELD, A., 1976, A comparative study of texture measures for terrain classification. *IEEE Transactions on Systems, Man, and Cybernetics*, **6**, 269–285.

WORNELL, G. W., 1995, *Signal Processing with Fractals: A Wavelet-based Approach* (Upper Saddle River, NJ: Prentice Hall).